

Pressure-Driven Quantum Criticality and T/H Scaling in the Icosahedral Au-Al-Yb Approximant

Shuya Matsukawa¹, Kazuhiko Deguchi¹, Keiichiro Imura¹, Tsutomu Ishimasa², and
Noriaki K. Sato^{1*}

¹*Department of Physics, Graduate School of Science, Nagoya University, Nagoya 464-8602, Japan*

²*Division of Applied Physics, Graduate School of Engineering, Hokkaido University, Sapporo 060-8628, Japan*

We report on ac magnetic susceptibility measurements under pressure of the Au-Al-Yb alloy, a crystalline approximant to the icosahedral quasicrystal that shows unconventional quantum criticality. In describing the susceptibility as $\chi(T)^{-1} - \chi(0)^{-1} \propto T^\gamma$, we find that $\chi(0)^{-1}$ decreases with increasing pressure and vanishes to zero at the critical pressure $P_c \simeq 2$ GPa, with $\gamma (\simeq 0.5)$ unchanged. We suggest that this quantum criticality emerges owing to critical valence fluctuations. Above P_c , the approximant undergoes a magnetic transition at $T \simeq 100$ mK. These results are contrasted with the fact that, in the quasicrystal, the quantum criticality is robust against the application of pressure. The applicability of the so-called T/H scaling to the approximant is also discussed.

Quantum phase transitions that occur at zero temperature have attracted much interest in the last decades. In some cases, unconventional superconductivity emerges in the vicinity of the quantum critical point (QCP) where the second-order transition temperature vanishes to zero. Experimentally, such a transition can be achieved by tuning an appropriate parameter such as pressure. Recent progress in material exploitation has revealed the emergence of a new class of quantum criticality that cannot be understood within the framework of conventional theories.¹⁻⁴

Such a typical example is found in the Tsai-type Au-Al-Yb icosahedral quasicrystal. Here, quasicrystals are metallic alloys that possess a nonperiodic yet long-range-ordered (quasiperiodic) arrangement of the atomic structure. As the temperature T is lowered toward zero, the physical properties diverge like $\chi \propto T^{-0.51}$ and $C_p/T \propto -\ln T$ (where χ is the magnetic sus-

*E-mail: kensho@cc.nagoya-u.ac.jp

ceptibility and C_p is the specific heat),⁵ suggesting that the system is just at the QCP without tuning.

In contrast, we found no divergence in the Au-Al-Yb approximant crystal, a crystalline phase whose unit cell has atomic decorations (i.e., Tsai-type clusters) that look like the quasicrystal (see Fig. 1 of Ref. 5). Magnetic susceptibility is described by $1/\chi - 1/\chi(0) \propto T^{0.51}$ [5], where the constant term $\chi(0)^{-1}$ ensures the absence of divergence, indicating that the system is away from the QCP.

The origin of the unusual low-temperature properties of the quasicrystal and the approximant is still controversial.^{4,6,7} Interestingly, these non-Fermi liquid features are similar to those of the heavy fermion crystals β -YbAlB₄ and YbRh₂Si₂.^{8–11} Therefore, further study of the Au-Al-Yb systems is helpful for obtaining a deeper understanding of quantum criticality in strongly correlated electron systems.

The quantum critical behavior of the quasicrystal is robust against the application of hydrostatic pressure (P). The divergence of magnetic susceptibility with the same critical index γ was observed even at $P = 1.54$ GPa,⁵ leading us to suggest the P - T phase diagram as schematically shown in Fig. 1(a). Instead of a quantum critical “point” in a conventional case, there seems to be a quantum critical “line” denoted by the thick line. This demonstrates that the quasicrystal is distinguished from conventional heavy fermion crystals in which there is a single QCP (or two QCPs as discussed below) and a tuning parameter is needed to control the distance from the QCP. In contrast, the approximant shows a nondiverging feature at ambient pressure; the susceptibility saturates at a finite value $\chi(0)$ with lowering temperature. However, it is yet unknown how the approximant behaves under pressure. Here, we study the high-pressure magnetic susceptibility of the approximant crystal and report the emergence of

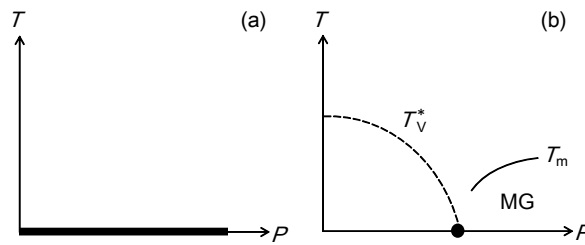


Fig. 1. Schematic P - T phase diagrams of the Au-Al-Yb quasicrystal (a) and approximant (b). The thick line in (a) indicates “a collection of QCPs”, which may be called the quantum critical line. The closed circle in (b) indicates the QCP. T_V^* is a characteristic temperature that is related to valence crossover.³ T_m and MG indicate a magnetic-ordering temperature and a magnetic ordered state, respectively.

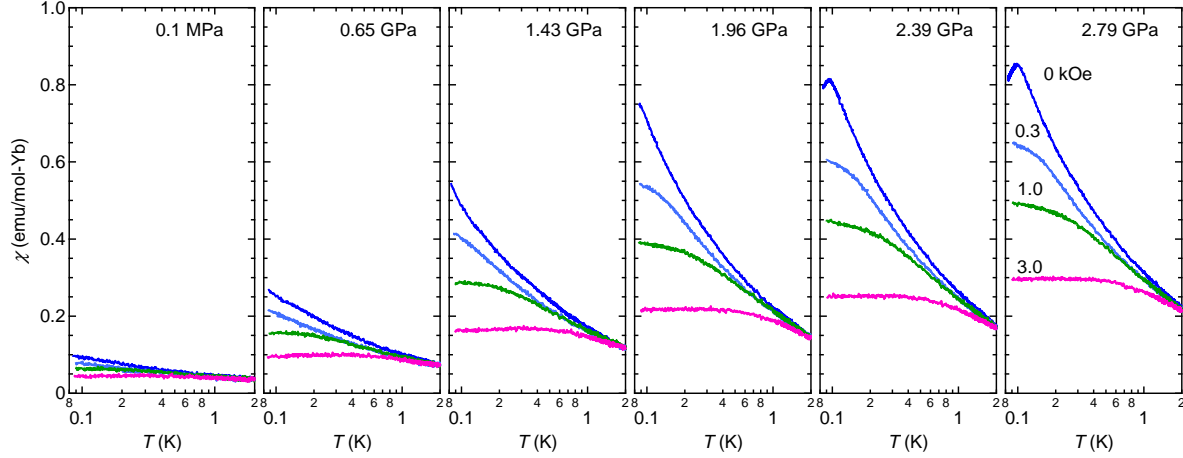


Fig. 2. (Color online) Temperature dependence of the ac magnetic susceptibility χ of the approximant crystal $\text{Au}_{49}\text{Al}_{36}\text{Yb}_{15}$ in a temperature range of $0.08 \lesssim T \lesssim 2$ K at pressures indicated. Applied dc magnetic fields are denoted in the figure of $P = 2.79$ GPa.

quantum criticality due to critical valence fluctuations at the critical pressure P_c , above which the magnetic ordering occurs [see Fig. 1(b)]. We also study the magnetic field effect on the criticality. It is known that the susceptibility is suppressed by the dc magnetic field at ambient pressure for both the approximant and the quasicrystal.⁵ Here, we report that the approximant shows a similar suppression of the susceptibility under pressure, which enables us to examine quantum criticality in terms of T/H scaling relations.

A 1/1 approximant crystal with the nominal composition, $\text{Au}_{49}\text{Al}_{36}\text{Yb}_{15}$, was prepared by arc-melting the starting materials, namely, 4N (99.99% pure)-Au, 5N-Al, and 3N-Yb, and subsequently annealing the obtained alloy ingot in an evacuated quartz ampoule at 750 °C for 116 h.¹² The ac magnetic susceptibility χ was measured by the conventional mutual inductance method. A modulation field with a frequency of 100.3 Hz and an amplitude of 0.1 Oe was superimposed on a dc magnetic field supplied by a superconducting magnet. For the calibration of the ac magnetic susceptibility, we measured the dc magnetization M using MPMS (Quantum Design) at pressures of up to 1.2 GPa, above which we extrapolated the dc magnetization data. Hydrostatic pressure was generated using a NiCrAl-BeCu piston cylinder cell for the measurement of ac susceptibility, together with Daphne oil 7373 as a pressure-transmitting medium. The pressure at low temperature was determined from the superconducting transition temperature of indium¹³ that was put into the pressure cell together with the sample.

Figure 2 shows the temperature dependence of the ac susceptibility, $\chi(T)$, of the Au-Al-

Yb approximant crystal under the dc magnetic field H and the hydrostatic pressure P . Here, $\chi(T)$ is the real part of the ac magnetic susceptibility. The low-temperature susceptibility for $H = 0$ strongly increases with pressure, whereas the application of the dc field suppresses this increase. At $P = 2.39$ and 2.79 GPa (the highest pressure of the present measurement), a peak structure is formed at $T_m \simeq 100$ mK for $H = 0$. It remains unknown whether this anomaly is associated with an antiferromagnetically long-range ordering or a spin-glass-like short-range ordering.

On the basis of the results obtained in Ref. 5 (see above), we assume the following modified Curie–Weiss relation for $H = 0$ except in a temperature region near T_m ;

$$\chi(T)^{-1} = T^{0.5}/C + \chi(0)^{-1}. \quad (1)$$

Here, the traditional Curie–Weiss plot where $1/\chi$ is a straight line as a function of T is replaced by a plot where $1/\chi$ is a straight line as a function of $T^{0.5}$ with the slope $1/C$ (where C is the Curie constant) and the vertical-axis intercept $\chi(0)^{-1}$. This straight-line feature is confirmed in Fig. 3(a) over a temperature range between about 85 mK (the base temperature of the experiment) and about 800 mK. (When evaluating the exponent γ as a free parameter, we obtain $\gamma = 0.50 \pm 0.05$ at ambient pressure and $\gamma = 0.50 \pm 0.01$ at $P = 1.96$ GPa.) Although the exponent γ does not depend on pressure, the intercept $\chi(0)^{-1}$ (that measures the distance from the QCP) approaches zero with increasing pressure. The latter observation is more clearly

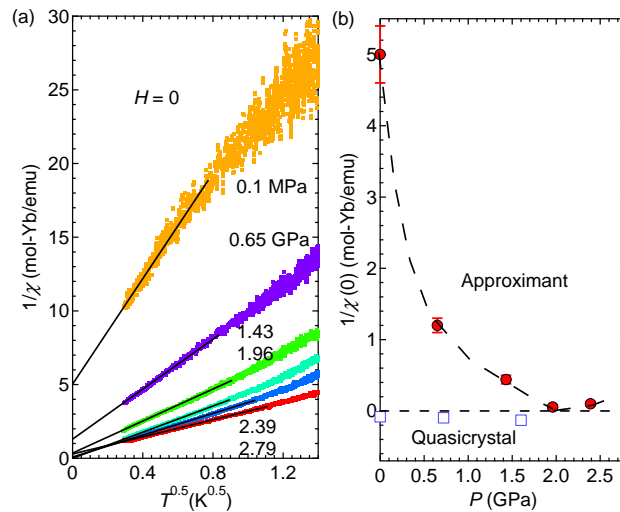


Fig. 3. (Color online) (a) Inverse magnetic susceptibility $1/\chi$ vs $T^{0.5}$ of the approximant $\text{Au}_{49}\text{Al}_{36}\text{Yb}_{15}$ at $H = 0$ under pressure ranging from ambient pressure to 2.79 GPa. The straight line indicates the extrapolation to zero temperature to evaluate $1/\chi(0)$. (b) Pressure dependence of $1/\chi(0)$ of the approximant (circles) and the quasicrystal (squares) at $H = 0$.

seen in Fig. 3(b): $1/\chi(0)$ steeply decreases with increasing pressure and vanishes at around 2 GPa, suggesting the emergence of the QCP there. This distinguishes the approximant from the quasicrystal in which $1/\chi(0) \sim 0$, independent of pressure, as indicated by the open square.⁵

It is now evident that the approximant is qualitatively different from the quasicrystal in the response to hydrostatic pressure, as schematically illustrated in Fig. 1. It seems reasonable to assume that this difference between the quasicrystal and the approximant is ascribed to the absence/presence of the periodicity. This is one of the primary results of this study.

In what follows, we study the magnetic field effect on the criticality. First, we examine the scaling properties of the ac susceptibility $\chi = \frac{dM}{dH}$. Let us start from the following uniform and static susceptibility that is deduced from the generalized susceptibility proposed for $\text{CeCu}_{6-x}\text{Au}_x$ by Schröder *et al.*,¹⁴

$$\begin{aligned}\chi^{-1}(H, T) &= \frac{1}{C} \left[\frac{1}{k_B^\alpha} \left((k_B T)^2 + (g\mu_B H)^2 \right)^{\alpha/2} + \theta^\alpha \right] \\ &= \frac{1}{C} \eta \left(\frac{H}{T} \right) T^\alpha + \frac{1}{C} \theta^\alpha,\end{aligned}\quad (2)$$

where k_B , g , μ_B , and θ are the Boltzmann constant, effective g -factor, Bohr magneton, and Weiss temperature, respectively. η is a scaling function of the ratio H/T only and equal to 1 for $H/T = 0$. The power index α was found to be 0.75 for $\text{CeCu}_{6-x}\text{Au}_x$. For the present system, we obtain $\alpha = 0.5$ by comparing Eq. (2) with the phenomenologically determined Eq. (1). (Note that $\eta = 1$ for $H = 0$.) Defining X as

$$X^{-1} = \chi^{-1} - \frac{\theta^{0.5}}{C}, \quad (3)$$

we obtain the scaling relation

$$XT^{0.5} = C\eta^{-1}. \quad (4)$$

At the QCP where $\chi(0)^{-1} = \theta^{0.5}/C = 0$, we have $X = \chi$ and hence the scaling relation

$$\chi T^{0.5} = C\eta^{-1}, \text{ at QCP.} \quad (5)$$

We plot $\chi T^{0.5}$ and $XT^{0.5}$ as functions of H/T in Figs. 4(a) and 4(b), respectively. In Fig. 4(a), we find that only the data of $P = 1.96$ GPa close to P_c collapse on a single curve, meaning that the scaling relation Eq. (5) holds in the present system. Equation (4) also holds because the data even at $P \neq P_c$ fall on a single curve, as seen in Fig. 4(b). Taking into account the fact that C depends on pressure [see Fig. 3(a)], we plot $XT^{0.5}/C$ in Fig. 4(c); although the ambient-pressure data scatter owing to their small susceptibility, all pressure data taken here fall on a single curve, which manifests that $XT^{0.5}/C$ is a function of H/T only.

Equation (4) is confirmed more quantitatively. According to the asymptotic form of the scaling function η^{-1} ,

$$\eta^{-1}\left(\frac{H}{T}\right) \sim \begin{cases} 1 - \frac{1}{4}\left(\frac{g\mu_B H}{k_B T}\right)^2, & \text{for } T \gg H, \\ \left(\frac{g\mu_B H}{k_B T}\right)^{-1/2}, & \text{for } T \ll H. \end{cases} \quad (6)$$

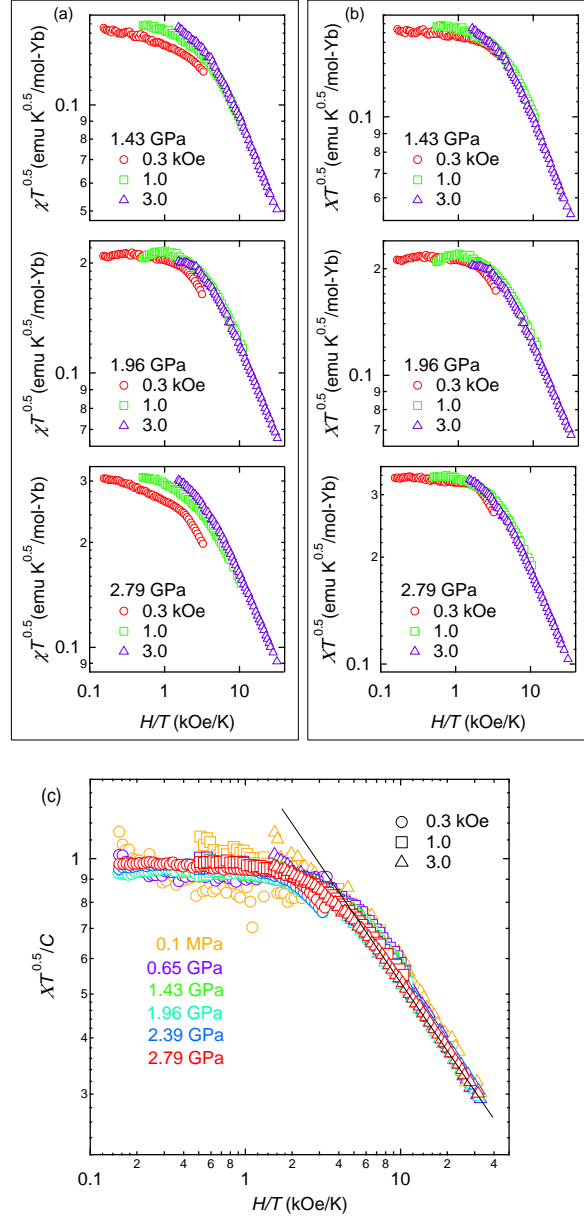


Fig. 4. (Color online) H/T scaling of the approximant $\text{Au}_{49}\text{Al}_{36}\text{Yb}_{15}$. The vertical axis denotes (a) $\chi T^{0.5}$, (b) $X T^{0.5}$, and (c) $X T^{0.5}/C$. (a) The scaling behavior observed at $P = 1.96$ GPa ($\simeq P_c$) becomes less evident as P moves away from P_c in either direction. (b) The critical component X satisfies the scaling relation even for $P \neq P_c$. (c) All the data fall on a single curve. The straight line indicates the Fermi liquid limit of the scaling function η^{-1} .

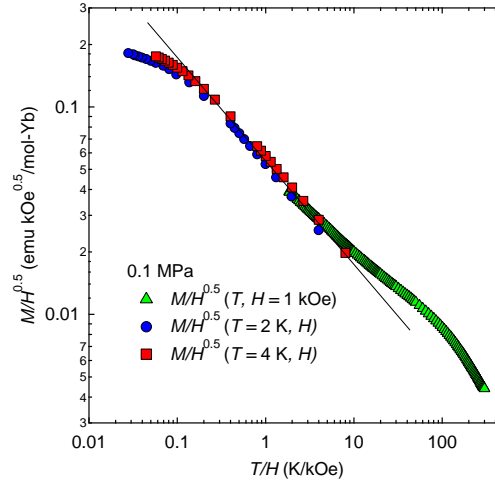


Fig. 5. (Color online) T/H scaling of dc susceptibility, $(M/H)H^{0.5}$, in a temperature interval between 2 K and room temperature. Note that the horizontal axis denotes T/H , instead of H/T in Fig. 4. Triangles indicate a temperature-sweep experiment, and circles and squares indicate a dc-field-sweep experiment at $T = 2$ and 4 K, respectively.

the data shown in Fig. 4(c) saturate at unity in the non-Fermi liquid limit ($H/T \ll 1$), while in the opposite limit of Fermi liquid ($H/T \gg 1$), they decrease linearly with increasing H/T . This indicates that the magnetic field drives the system to the Fermi liquid regime.

Next, we discuss that the unusual exponent $\alpha = 0.5$ obtained above can be deduced from the following low-temperature free energy, which was proposed for the analysis of the quantum criticality of β -YbAlB₄ by Matsumoto *et al.*,⁹

$$F = -\frac{1}{(k_B \tilde{T})^{1/2}} \left[(g\mu_B H)^2 + (k_B T)^2 \right]^{3/4}, \quad (7)$$

where \tilde{T} is a characteristic temperature. By differentiating F with respect to H , we obtain the ac susceptibility and the dc susceptibility M/H (where M is a magnetization) as

$$\chi(T, H)T^{1/2} = \psi\left(\frac{H}{T}\right), \quad \text{for } H \geq 0, \quad (8)$$

$$\frac{M}{H}H^{1/2} = \varphi\left(\frac{T}{H}\right), \quad \text{for } H > 0, \quad (9)$$

where ψ and φ are scaling functions, and $\psi = \frac{3}{2} \frac{(g\mu_B)^2}{k_B \tilde{T}^{1/2}}$ for $H = 0$. Equation (8) is equivalent to Eq. (5) when $C\eta^{-1} = \psi$, and a comparison of Eq. (8) with Eq. (2) yields $\alpha = 0.5$.

Then, we test the scaling relation Eq. (9) for the dc magnetization using data taken at high temperatures ($2 \text{ K} \lesssim T \lesssim \text{room temperature}$) and high dc fields ($H \lesssim 70 \text{ kOe}$) (see Fig. 5). (We used the ambient-pressure data instead of the high-pressure one because the high-pressure magnetization contains a non-negligible contribution from the pressure cell and

it was difficult to accurately separate the sample magnetization from the total magnetization.) For $T/H > 10$ (i.e., $T > 10$ K for $H = 1$ kOe), we find a deviation from the expected behavior (denoted by the thin line) from the asymptotic form

$$\varphi\left(\frac{T}{H}\right) \sim \frac{3(g\mu_B)^{3/2}}{2(k_B\tilde{T})^{1/2}} \left(\frac{k_B T}{g\mu_B H}\right)^{-1/2}, \text{ for } T \gg H. \quad (10)$$

This is ascribed to the crystal field effect because the $4f$ electrons are localized at high temperatures as evidenced by the conventional Curie–Weiss behavior in $\chi(T)$.^{5,15}

It is now clear that the T/H scaling holds (except in the very high temperature region) in the approximant like $\text{CeCu}_{6-x}\text{Au}_x$ and $\beta\text{-YbAlB}_4$. We note that the same scaling is also applicable to the Au–Al–Yb quasicrystal (not shown here). In all four systems, therefore, the critical field H_c of the quantum phase transition is zero because a finite H_c would require that the argument of the scaling functions is the ratio $T/|H - H_c|$.⁹ This may lead to a similar H – T phase diagram for those systems. In contrast, the P – T phase diagram strongly depends on the system as demonstrated in Fig. 1; for $\text{CeCu}_{5.8}\text{Au}_{0.2}$ and $\beta\text{-YbAlB}_4$, see Refs. 16 and 17, respectively.

Let us discuss a possible origin of the QCP. As presented above, the uniform susceptibility shows the power law divergence with the critical index $\gamma \simeq 0.5$ at $P = P_c$. This divergence cannot be understood from the conventional magnetic QCP because the high-pressure magnetic state is not ferromagnetic but antiferromagnetic (or spin-glass-like). Instead, the divergence with the above critical index can be explained by the critical valence fluctuation model proposed by Watanabe and Miyake.¹⁸ Remembering that the valence in the present system fluctuates between Yb^{2+} and Yb^{3+} as evidenced by X-ray absorption experiments¹⁹ and photoemission experiments,²⁰ we suggest that the QCP arises from the critical valence fluctuations. This interpretation is supported by the theoretical suggestion that the scaling relation Eq. (9) is deduced from the critical valence fluctuation model.²¹

Finally, we comment on the P – T phase diagram of the approximant. In Fig. 1(b), we plot the valence-fluctuation QCP. We found the emergence of the magnetic (short-range or long-range) ordering state at pressures above P_c . Therefore, it is possible that there is another QCP of magnetic origin at which T_m vanishes. The interplay between magnetic and valence instabilities was predicted using the critical valence fluctuation model,³ and was observed experimentally in YbNi_3Ga_9 .²² To compare these results with the present system, a detailed P – T phase diagram of the approximant should be constructed.

In summary, we measured the ac magnetic susceptibility of the approximant crystal

$\text{Au}_{49}\text{Al}_{36}\text{Yb}_{15}$. As $T \rightarrow 0$, the uniform susceptibility diverges at the critical pressure $P_c \simeq 2$ GPa, which we ascribed to the critical valence fluctuations. At pressures above P_c , the magnetic transition occurs at $T_m \simeq 100$ mK, although it remains to be revealed in the future whether this transition is of long- or short-range nature. This pressure effect is remarkably contrasted with the robustness of the quantum criticality in the quasicrystal against the application of pressure, which we ascribe to the difference in the presence/absence of the periodicity. For the magnetic field effect, on the other hand, the approximant satisfies the T/H scaling applied to $\text{CeCu}_{6-x}\text{Au}_x$ and $\beta\text{-YbAlB}_4$, meaning that there is no critical field H_c . In conclusion, we found that the pressure and magnetic field play different roles in quantum criticality.

The authors thank Yukinori Tanaka and Shin Yamamoto for support of the experiments, and Kazumasa Miyake for careful reading of the manuscript. This work was financially supported by a Grant-in-Aid for Scientific Research from JSPS, KAKENHI (Nos. 26610100, 15H02111, and 15H03685) and Program for Leading Graduate Schools “Integrative Graduate Education and Research Program in Green Natural Sciences”, MEXT, Japan, and also by Toyota Physical & Chemical Research Institute.

References

- 1) Q. Si, S. Rabello, K. Ingersent, and J. L. Smith, *Nature* **413**, 804 (2001).
- 2) M. Imada, T. Misawa, and Y. Yamaji, *J. Phys.: Condens. Matter* **22**, 164206 (2010).
- 3) S. Watanabe and K. Miyake, *J. Phys.: Condens. Matter* **23**, 094217 (2011).
- 4) S. Watanabe and K. Miyake, *J. Phys. Soc. Jpn.* **82**, 083704 (2013).
- 5) K. Deguchi, S. Matsukawa, N. K. Sato, T. Hattori, K. Ishida, H. Takakura, and T. Ishimasa, *Nat. Mater.* **11**, 1013 (2012).
- 6) V. R. Shaginyan, A. Z. Msezane, K. G. Popov, G. S. Japaridze, and V. A. Khodel, *Phys. Rev. B* **87**, 245122 (2013).
- 7) E. C. Andrade, A. Jagannathan, E. Miranda, M. Vojta, and V. Dobrosavljevic, *Phys. Rev. Lett.* **115**, 036403 (2015).
- 8) S. Nakatsuji, K. Kuga, Y. Machida, T. Tayama, T. Sakakibara, Y. Karaki, H. Ishimoto, S. Yonezawa, Y. Maeno, E. Pearson, G. G. Lonzarich, L. Balicas, H. Lee, and Z. Fisk, *Nat. Phys.* **4**, 603 (2008).
- 9) Y. Matsumoto, S. Nakatsuji, K. Kuga, Y. Karaki, N. Horie, Y. Shimura, T. Sakakibara, A. H. Nevidomskyy, and P. Coleman, *Science* **331**, 316 (2011).
- 10) O. Trovarelli, C. Geibel, S. Mederle, C. Langhammer, F. M. Grosche, P. Gegenwart, M. Lang, G. Sparn, and F. Steglich, *Phys. Rev. Lett.* **85**, 626 (2000).
- 11) P. Gegenwart, T. Westerkamp, C. Krellner, Y. Tokiwa, S. Paschen, C. Geibel, F. Steglich, E. Abrahams, and Q. Si, *Science* **16**, 969 (2007).
- 12) T. Ishimasa, Y. Tanaka, and S. Kashimoto, *Phil. Mag.* **91**, 4218 (2011).
- 13) L. D. Jennings and C. A. Swenson, *Phys. Rev.* **112**, 31 (1958).
- 14) A. Schröder, G. Aeppli, R. Coldea, M. Adams, O. Stockert, H. v. Löhneysen, E. Bucher, R. Ramazashvili, and P. Coleman, *Nature* **407**, 351 (2000).
- 15) S. Matsukawa, K. Tanaka, M. Nakayama, K. Deguchi, K. Imura, H. Takakura, S. Kashimoto, T. Ishimasa, and N. K. Sato, *J. Phys. Soc. Jpn.* **83**, 034705 (2014).
- 16) O. Stockert, F. Huster, A. Neubert, C. Pfleiderer, T. Pietrus, B. Will, and H. v. Löhneysen, *Physica B* **312-313**, 458 (2002).
- 17) T. Tomita, K. Kuga, Y. Uwatoko, P. Coleman, and S. Nakatsuji, *Science* **349**, 506 (2015).
- 18) S. Watanabe and K. Miyake, *Phys. Rev. Lett.* **105**, 186403 (2010).

-
- 19) T. Watanuki, S. Kashimoto, D. Kawana, T. Yamazaki, A. Machida, Y. Tanaka, and T. J. Sato, Phys. Rev. B **86**, 094201 (2012).
- 20) M. Matsunami, A. Chainani, M. Taguchi, M. Oura, S. Shin, T. Hajiri, S. Kimura, T. Takeuchi, K. Tamasaku, Y. Tanaka, T. Ishikawa, T. Ebihara, K. Imura, K. Deguchi, N. K. Sato, and T. Ishimasa, unpublished.
- 21) S. Watanabe and K. Miyake, J. Phys. Soc. Jpn. **83**, 103708 (2014).
- 22) K. Matsubayashi, T. Hirayama, T. Yamashita, S. Ohara, N. Kawamura, M. Mizumaki, N. Ishimatsu, S. Watanabe, K. Kitagawa, and Y. Uwatoko, Phys. Rev. Lett. **114**, 086401 (2015).